CrystEngComm

PAPER

View Article Online
View Journal | View Issue

Cite this: *CrystEngComm*, 2018, **20**, 7582

One-step synthesis of non-symmetric CuI nanoplates for a highly sensitive non-enzymatic glucose biosensor†

Misbah Ullah Khan,[ab] Hongjun You,*[ab] Dongjie Zhang,[b] Lingling Zhang[b] and Jixiang Fang*[b]

Received 18th August 2018,
Accepted 2nd November 2018

DOI: 10.1039/c8ce01387j

rsc.li/crystengcomm

The construction of active nanomaterials on the surface of electrodes is very useful to boost electrochemical properties. Recently, great focus has been given to obtain immensely sensitive and selective glucose biosensors. This study demonstrates the well-controlled synthesis of non-symmetric two dimensional CuI nanoplates *via* a facile one-pot method in aqueous solution. On one side, the surface of the uniform non-symmetrical CuI nanoplates is covered with teeth-like tips, and on the other side the surface is flat and smooth. The non-symmetrical CuI nanoplate displays very high sensitivity properties in structure-dependent ultra-sensitive non-enzymatic glucose biosensors with a wide linear range, which could be ascribed solely to the non-symmetrical structural morphology. This novel study may perhaps open an innovative way to promote non-enzymatic glucose sensing properties.

Introduction

The construction of glucose biosensors with ultra-high sensitivity has been given attention due to their outstanding applications in different areas such as medical analysis, diabetes management, bioprocess monitoring, food production and environmental intensive care.[1–4] On a universal basis, the number of people affected by diabetes is around 382 million, and will reach half a billion by the year 2035.[5] People suffering from diabetes are at a higher risk of many diseases such as heart problems, blindness and kidney failure, caused by an unsuitable amount of insulin.[6,7] By advancing nanomaterials in the biomedical field, the utilization of self-controlled devices will have a significant impact on the healthcare industry.[8–10] A key point to ensure the reliability and sensitivity of biological and chemical detection focuses on the fabrication of uniform and highly sensitive devices.[11–13] Several techniques based on electrochemistry, photosensitive measurements, exterior plasmon resonance and capacitive recognition have been developed for the detection of glucose concentration in blood.[14–16] Consequently, in clinical detection of diabetes, more attention is given to glucose blood concentration.[17] The catalytic oxidation of glucose to bound gluconolactone, producing H_2O_2,[7] has led people to develop electrochemical sensing methods. The electrochemical reaction of H_2O_2 possesses sensitivity and selectivity, which can be used to estimate glucose concentration.[18,19] Still, variability, complex control techniques and the great price of enzymatic glucose biosensors severely slow down mass use of these sensors. Hence, it is very important to prepare such types of biosensor which have excellent stability and performance.[20]

Among all metal materials, copper-based non-enzymatic glucose sensors have been given more attention due to their low cost, excellent electrochemical activity and high specific surface area compared to other metal nanomaterial-based non-enzymatic glucose sensors.[21] In the past few decades, because of their low cost and high selectivity, many studies have been reported to better improve glucose sensors such as those based on CuO nanowires, nanoporous CuO/Cu, Nafion/Cu_2O, SLNs/Ag/Si, Cu_xO/Cu, Cu nanowires, GO/CuO/GCE, Cu_xO nanosheets/Cu and so on.[22,23] Other reported sensors are for instance ZnO-based, where the effect of Schottky-gated devices is higher than ohmic contact devices, since particles at the intersection locale can change the "gate" that viably tunes conductance.[24] An adaptable self-controlled ultrasonic power sensor, in view of tribo-electric dynamic sensors, demonstrated astoundingly long performance with low cost.[25] The latest reports of persistent non-enzymatic glucose sensors are based on nanomaterials, in spite of numerous challenges modelled through these glucose sensors.[26] Unfortunately, practical applications of the reported non-enzymatic

[a] *School of Science, Xi'an Jiaotong University, Shaanxi 710049, P.R. China. E-mail: hjyou@mail.xjtu.edu.cn*
[b] *Key Laboratory of Physical Electronics and Devices of Ministry of Education, School of Electronic and Information Engineering, Xi'an Jiaotong University, Xi'an, Shaanxi 710049, P.R. China. E-mail: jxfang@mai.xjtu.edu.cn*

† Electronic supplementary information (ESI) available: EDX analysis, PXRD patterns and amperometric current–time response for the CuI nanoflowers and CuI microparticles. See DOI: 10.1039/c8ce01387j

glucose sensors based on numerous kinds of nanomaterial such as metals,[27,28] metal oxides,[29,30] metal alloys,[31,32] and metals complexes[33] *etc.* are limited. The limitation of these non-enzymatic glucose sensors comes from their high cost, and low selectivity and sensitivity.

We know that structure-based novel nano-architecture always enhances certain properties of nanomaterials, such as the band alignment of non-symmetric structures. The introduction of Ti at a TiO_2/Au film interface has been tuned, thereby promoting separation of photo-generated carriers *via* the efficient transport of electrons to the Au film.[34,35] Furthermore, enhanced sensitivity of nanostructures arises from modification of the overall dissymmetric factors to increase the electric field strength for nano-focusing.[36] The non-symmetric nanostructures, which were composed of Ag nanoparticles hanging inside or capping the top of ZnO hollow nanospheres, allowed the generation of a strong local electric field near the contact area owing to a non-symmetric dielectric environment.[37] Similarly, simulation and analysis of an asymmetric nanostructure optimized the resonance and enhanced the properties of nanoantennas.[38] This is similar to our previous report on Ag/AgI nanoplates, where one side was rough and the other side was smooth, with Ag NPs non-symmetrically distributed on one side of AgI nanoplate, which enhanced the photocatalytic properties.[39]

In this work, we developed non-enzymatic sensors based on the growth of CuI nanoplates, CuI nanoflowers and CuI microparticles *via* a one-pot synthesis in aqueous solution. Due to their novel non-symmetric nanostructure, the CuI nanoplates show greatly enhanced sensitivity as electrochemical glucose sensors. To the best of our knowledge, CuI-based electrochemical glucose sensors are reported for the first time. To inspect the linear range sensitivity, the properties were measured by cyclic voltammetry (CV) experiments and chronoamperometry (CA) . Electrochemical impedance spectroscopy (EIS) was also used for a linear range sensitivity investigation, demonstrating that the CuI nanoplates have better properties than CuI nanoflowers and CuI microparticles.

Methods

Materials

The chemicals used were polyvinylpyrrolidone (PVP, average MW 58 000, Aladdin chemical reagent), copper chloride ($CuCl_2{\cdot}2H_2O$, Tianli Chemical Reagent Co, LTD, 99%), potassium iodide (KI, Guangdong Guanghua Sci-Tech Co, LTD, 99.5%), glucose ($C_6H_{12}O_6{\cdot}H_2O$, Tianli Chemical Reagent Co, LTD, 99%), potassium chloride (KCl, Tianjin Hongyan Chemical Reagent Factory, 99%), potassium ferric cyanide ($K_3[Fe(CN)_6]$, Tianli Chemical Reagent Co, LTD, 99%), and sodium hydroxide (NaOH, Guangdong Guanghua Sci-Tech Co, LTD, 99.5%). All of the chemicals used in this study were of analytical grade, and the solutions were made in deionized water (DI) obtained from a Millipore system.

Synthesis of CuI nanostructures

The CuI nanostructures were synthesized by a simple method in aqueous solution. For the construction of the CuI nanoplates, 9 mL of DI water, 10 mg of copper chloride ($CuCl_2{\cdot}2H_2O$) and 160 mg of PVP were added to a 20 mL flask. To mix well, the flask containing the solution was equipped with a magnetic stirrer bar, with a constant speed of 400 rpm for a time period of 4 min. In the next step, 150 μL of KI aqueous solution (1 M) was poured into the flask and stirred for 10 min at room temperature to make the solution homogenous. In the third stage, the flask was placed into an oil bath at 140 °C with for a time period of 90 min, keeping the magnetic bar speed at 400 rpm. Finally, the product was separated from the solution *via* centrifugation at a speed of 10 000 rpm for a time period of 10 min, then washed twice with a water/ethanol mixture and once with ethanol. To construct the CuI nanoflowers and microparticles, all of the parameters were kept same except for the concentration of copper chloride. The CuI nanoflowers and the CuI microparticles were obtained with 4 mM and 6 mM copper chloride, respectively.

Characterizations

The morphologies of the prepared products (CuI nanoplates, CuI nanoflowers, and CuI microparticles) were characterized with a field emission scanning electron microscope (FE-SEM) (JEOL JSM-7000F) and a transmission electron microscope (TEM) (JEOL JEM-3010). The energy dispersive X-ray (EDX) investigation was achieved with an Oxford INCA detector installed on the SEM. Powder X-ray diffraction (PXRD) spectra were obtained using a BRUKER D8 ADVANCE X-ray diffractometer with a Cu Kα X-ray source (λ = 1.5405 Å).

Electrochemical properties measurements

A glassy carbon electrode with a diameter of 5 mm, with CuI nanoplate, CuI nanoflower and CuI microparticle products on its surface with an equal concentration of 15 μl (1 mM) was used as the working electrode with 10 μl of Nafion binder (0.025 wt%) as an additive. The electrochemical tests were performed at room temperature in a typical three-electrode system (CHI-760C, Shanghai Chenhua, China) in which Ag/AgCl and Pt foil were used as the reference electrode and the counter electrode, respectively. Cyclic voltammetry (CV) and chronoamperometry (CA) measurements were performed in 100 mL of 0.1 M KOH aqueous solution with certain concentrations of glucose. Amperometric examinations were performed under constant magnetic stirring to guarantee that glucose and the electrolyte (KOH solution) were entirely mixed. Electrochemical impedance spectroscopy (EIS) experiments were accomplished in the presence of 5 mM $K_3[Fe(CN)_6]$ with 0.1 M KCl as the assistant electrolyte.

Results and discussion

The CuI nanoplates were synthesized *via* a one-pot method in solution which is modest but robust. Copper chloride ($CuCl_2 \cdot 2H_2O$) was reacted with KI to form CuI in the presence of polyvinylpyrrolidone (PVP). The morphology and structures of the as-prepared CuI nanoplates are shown in Fig. 1. The SEM image of the CuI nanoplates with a uniform morphology across a large area is shown in Fig. 1a. The high magnification SEM image in Fig. 1b shows tooth-like shapes on the surface of the CuI nanoplate. Furthermore, the magnified image obtained from the circled area indicates that the two dimensional (2D) CuI nanoplate possesses a novel non-symmetric structure. One side of the 2D nanoplates is rough with tooth-like shapes and the other side is flat and smooth. As shown in Fig. 1c, the side-view image of a single tooth-like tip shows a triangular shape, and the thickness of the 2D nanoplates was around 27 nm. Because of the non-symmetric structure, the CuI nanoplate shows different morphology from different perspectives. So, from the top view, it shows a rough surface; from the bottom view, it shows a smooth surface; and from the side view it shows the teeth-like shape. Thus, from Fig. 1a–c we can find that the shapes of CuI nanoplates are the same, but their size is different somehow. The sizes of the small nanoplates are around 100 nm, and the large ones are around 200–300 nm. Fig. 1d shows the TEM image of the top side of single CuI nanoplates. Each tooth-like tip shows a triangular projection shape, with the length of the side being around 20–30 nm, which is close to the thickness of the nanoplates. From the images, both from the side view and the top view, it can be deduced that the CuI nanoplates are formed by the connection of tetrahedral subunits in two-dimensional space. Dependent on these results, the morphology of the non-symmetric CuI nanoplates is clearly illustrated by the schematic image in Fig. 1f. Although the CuI nanoplate is constructed from plenty of tetrahedral subunits, it is still a single crystal as detailed by the selected area electron diffraction (SAED) patterns (Fig. 1e).

EDX analysis for the non-symmetric CuI nanoplates is shown in Fig. S1.† The ratio between the Cu and I atoms is nearly 1 : 1, matching well with the ratio for the CuI molecular structure. Furthermore, the obtained products were examined by their PXRD patterns (Fig. S2†). The diffraction peaks of PXRD were well indexed, agreeing with the standard structure of CuI crystals (space group: $F\bar{4}3m$, crystal system: cubic, JCPDS file No. 01-083-1105). The crystalline structure of CuI was confirmed from the PXRD pattern, showing that there were no other elements found such as copper or cupric oxide.

The formation process of the non-symmetric CuI nanoplates was examined by characterizing the product obtained during different reaction times in the synthesis system. The SEM images of the CuI products with a synthesis time of 5, 10, 30, and 90 minutes are shown in Fig. 2a–d, respectively.

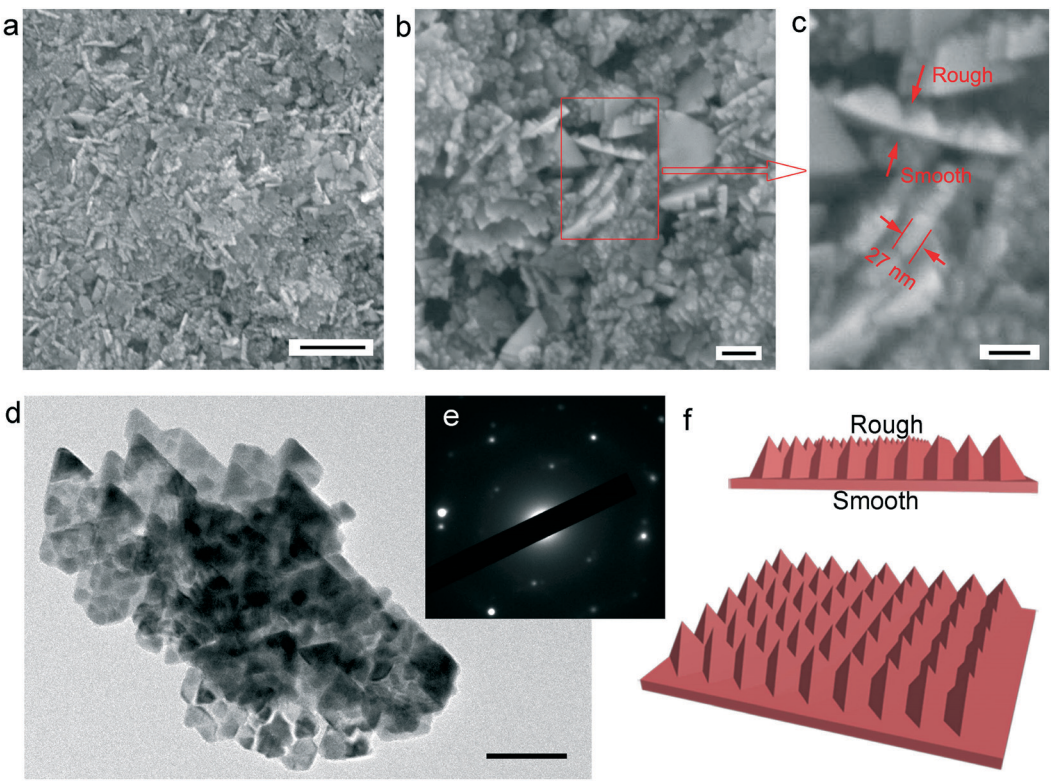

Fig. 1 The (a) low and (b) high magnification SEM images of the CuI nanoplates. (c) The SEM image magnified from the circled area in (b). (d) The TEM image and (e) the corresponding SAED pattern for the CuI nanoplates. (f) Schematic images to illustrate the morphology of the non-symmetric CuI nanoplates. The scale bars in (a–d) are 500 nm, 100 nm, 50 nm, and 100 nm, respectively.

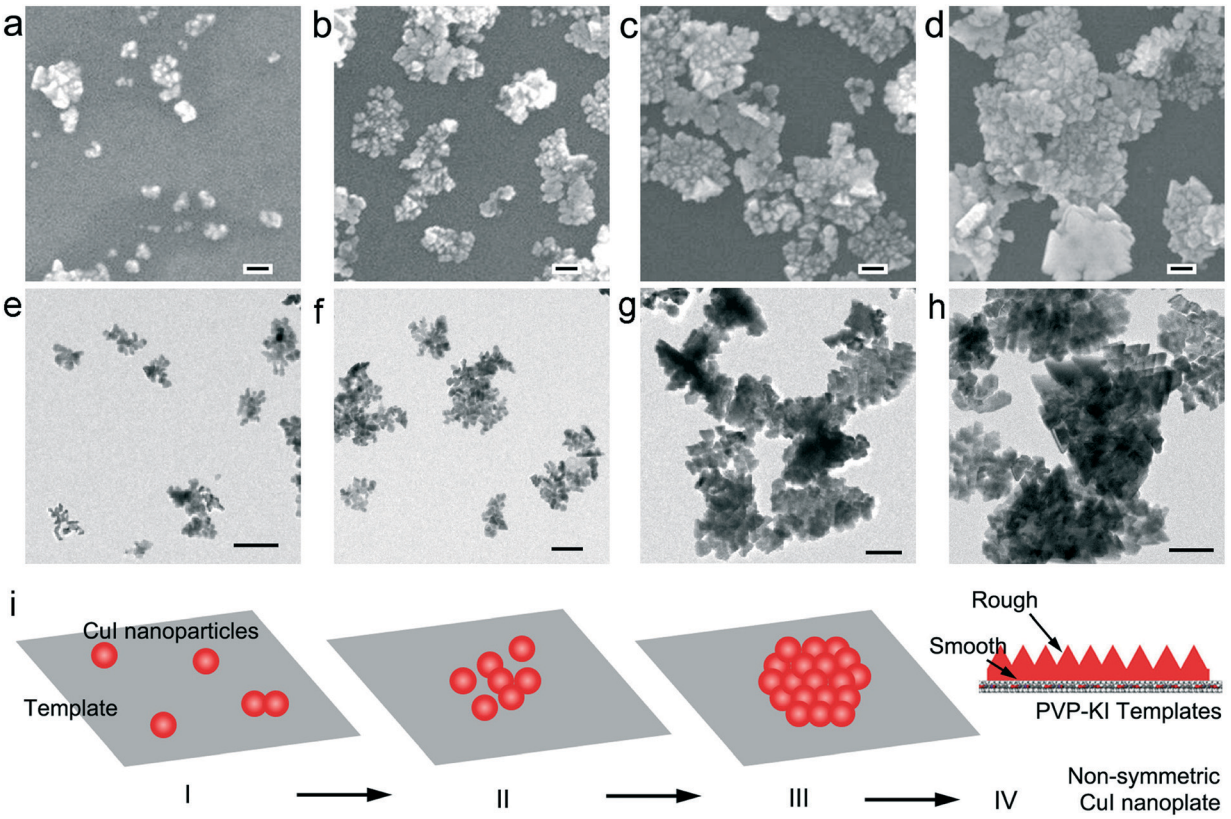

Fig. 2 SEM images and a schematic diagram for the formation process of the CuI-nanoplates. (a–d) SEM images of the CuI nanoplates synthesized with different reaction times: 5, 10, 30, and 90 min. The scale bars in (a–d) are 100 nm. (e–h) TEM images of the CuI nanoplates synthesized with different reaction times: 5, 10, 30, and 90 min. The scale bars in (e–h) are 200 nm. (i) Schematic image for the formation of CuI nanoplates on the 2D PVP–KI soft template.

The construction of the CuI nanoplates are shown schematically in Fig. 2e, which was assumed from the experimental results. Referring to the growth of non-symmetric ZnO nanodisks with bis(2-ethylhexyl) sulfosuccinate (NaAOT) assisting as a soft template,[40] non-symmetric Au nanoplates with PEG–water as a soft template,[41] and non-symmetric Ag/AgI nanoplates with EG-KI as a soft template,[39] here, we deduced the soft template being formed between PVP and KI molecules, limited by the two dimensional PVP–KI soft template. To further clarify the growth process of the CuI nanoplates, TEM analyses were performed, shown in Fig. 2e–h. The growth process of CuI is illustrated in Fig. 2i. In the preliminary stage, CuI nuclei and nanoparticles (NPs) are created and favourably develop on the surface of the PVP–KI soft template. In the subsequent stage, through a particle-mediated evolution procedure as reported in previous papers,[42–44] CuI NPs contact each other on the surface of the soft template. With more CuI NPs aggregated together, two dimensional nanoplates are formed on the surface of the soft template. In the last step, the CuI nanoplates perform an over growth and ripening process based on an atom-mediated growth mode.[44,45] The growth of the CuI nanoplates is limited by the two-dimensional soft template. One side of the nanoplate which is covered by the soft template is smooth. The other side of the nanoplate not being covered by the soft templates forms the tooth-like morphology. PVP is the key factor in the formation of the soft template. In the formation process of the CuI nanoplates, the soft template is firstly formed between PVP and KI, and then the growth occurs on the surface of the soft template. Without the use of PVP, there was no formation of the soft template and no two dimensional nanoplates could be obtained without the limitation of the soft template, even using the same experimental conditions. The corresponding SEM images of the CuI particles synthesized without PVP are shown in Fig. S3†, with variation of the copper chloride concentration from 2 mM to 4 mM to 6 mM.

The effect of the concentration of Cu^{2+} ions on the morphology of the CuI nanostructure was investigated. When the copper chloride ($CuCl_2{\cdot}2H_2O$) precursor was increased to an excess compared to the quantity of KI, with all of the other experimental conditions kept constant, the same thin sized CuI nanoplates were rounded, turning the morphology from CuI nanoplates to CuI nanoflowers. It was observed that when the precursor concentration was changed from 2 to 4 mM, CuI nanoflowers were obtained, and when it was further changed to 6 mM, CuI microparticles were obtained, as shown in Fig. 3. EDX analysis and PXRD analysis of the CuI nanoflowers and the CuI microparticles are shown in Fig. S4–S6,† which have the same result as that of the CuI nanoplates, indicating that they possess the same crystalline

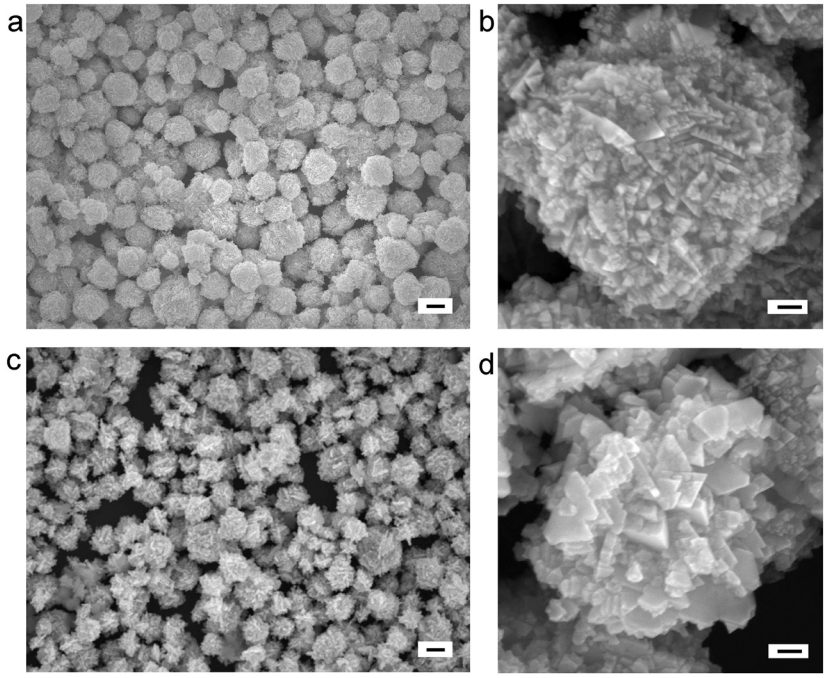

Fig. 3 (a) Low and (b) high magnification SEM images of the CuI nanoflowers, and (c) low and (d) high magnification SEM images of the CuI microparticles, respectively. The scale bars in (a) and (c) are 1 μm, and in (b) and (d) are 100 nm.

structure and composition. The low and high magnification images of the CuI nanoflowers in Fig. 3a and b show that the nanoflowers were formed by the aggregation of the CuI nanoplates. Compared to the CuI nanoflowers, the size of the whole particle was similar, while the nano-projection on the CuI microparticles was larger, as shown in Fig. 3c and d.

The potential application of the CuI nanostructures synthesised in our system as sensor materials was investigated for the non-enzymatic detection of glucose. To investigate the CuI crystal-based electrodes and the catalytic activity of glucose, cyclic voltammetry (CV) measurements were performed. Fig. 4a shows the CV curves of the CuI nanoplate-centred electrodes. To perform the CV measurements the conditions were kept as: 0.1 M KOH solution, with varying glucose concentration (0 to 5 mM), a scan rate of 50 mV s^{-1} and maintaining a vertex potential (0 to 0.8 V). From the CV curves shown in Fig. 4a, at a 0 mM glucose concentration there was no oxidation current, and by increasing the concentration of glucose the oxidation current was gradually increased and had a maximum response at a 5 mM glucose concentration. Fig. 4b and c are the CV curves of the CuI-nanoflowers and CuI-microparticles under the same measurement conditions as the CuI nanoplates. The amperometric response signals also increased with an increase of glucose concentration, similar to that of the CuI nanoplates, but the currents of the CuI-nanoflowers and CuI-microparticles were much lower than that of the CuI nanoplates. Moreover, the oxidation peak of glucose at around 0.55 V was obviously shown in the CV curves of the CuI nanoplates, while the oxidation peak in the CV curves of CuI-nanoflowers and CuI-microparticles was not clear, indicating that the CuI nanoplates significantly increased the electrochemical catalytic

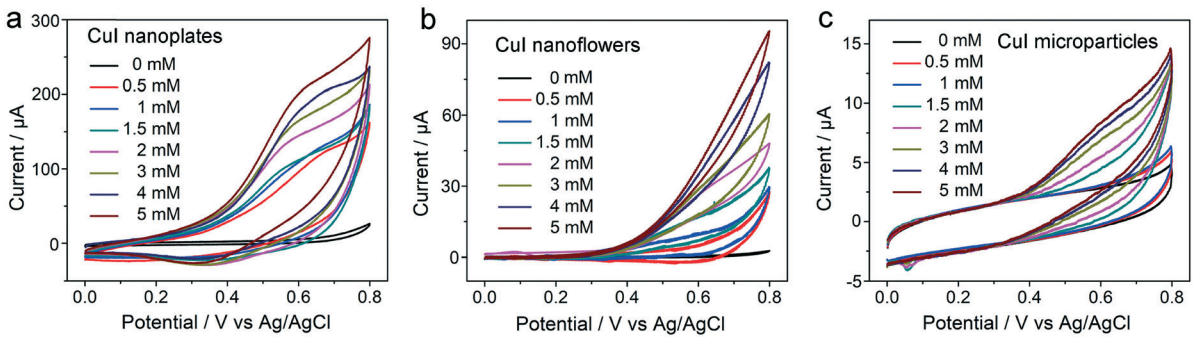

Fig. 4 The cyclic voltammetry (CV) curves of the (a) CuI nanoplates, (b) CuI nanoflowers and (c) CuI microparticles with different glucose concentrations from 0 to 5 mM with 0.1 M KOH solutions at a scan rate of 50 mV s^{-1}.

performance of the electrode and raised the electrocatalytic capacity in the direction of glucose oxidation.

From the CV curves, it was seen that by increasing the concentration of glucose, the CuI crystals enabled the transfer of electrons from the working electrode and glucose, resulting in a gradual increase in voltage from 0 to 0.8 V which was followed by the redox couple.[46] For the CuI nanoplate-modified electrode, the electron transfer was faster than the CuI nanoflowers and CuI microparticles, which increased the rate of electrocatalytic activity. The whole mechanistic process for the oxidation of glucose is shown as follows for the CuI electrodes.[47]

$$\mathrm{Cu(I)} + \mathrm{OH^-} \rightarrow \mathrm{Cu(II)} + \mathrm{e} \quad (1)$$

$$\mathrm{Cu(II)} + \mathrm{OH^-} \rightarrow \mathrm{Cu(III)} + \mathrm{e} \quad (2)$$

$$\mathrm{Cu(III)} + \text{glucose} + \mathrm{e} \rightarrow \mathrm{Cu(II)} + \text{gluconic acid} + \mathrm{OH^-} \quad (3)$$

$$\mathrm{Cu(III)} + \text{glucose} + \mathrm{e} \rightarrow \mathrm{Cu(I)} + \text{gluconic acid} + \mathrm{OH^-} \quad (4)$$

From eqn (1), at the start under alkaline conditions the Cu(I) of CuI was converted to Cu(II).[48] A further oxidation process took place on the surface of the electrodes and Cu(II) was oxidized to Cu(III), as shown in eqn (1) and (2). Eqn (3) and (4) show the continuous electrochemical oxidation of glucose to gluconic acid with the assistance of Cu(II) and Cu(III), resulting in the simultaneous reduction of Cu(III) and Cu(II) to Cu(II) and Cu(I) which is shown in eqn (3) and (4). The construction of Cu(III) tips and high catalytic measurements of the formation of the Cu(III) species led to a boost in catalytic current due to the oxidation of glucose, and as a result an electron was transferred between glucose and the working electrode. In this case, the formation of the Cu(III) species was possible, and was the main source for electron transfer as a medium for glucose oxidation. Thus, by increasing the glucose concentration, the catalytic current response was also increased in the presence of the CuI crystal-modified electrode.

Fig. 5a, displays amperometric curves of the CuI nanoplate-modified electrode through continuous addition of glucose into 0.1 M NaOH solution, where the functional voltage was +0.62 V. Meanwhile, stirring was introduced to obtain a solution of glucose identical to that of the electrolyte. As shown in Fig. 5a, the CuI nanoplate electrode showed an evident current response at 0.5 mM glucose concentration. When the concentration of the step-wise addition of glucose was 0.5 mM, a prompt increase was shown with the addition of more glucose. The CuI nanoplate-modified electrode displayed a step-like boost in accordance with an increase in glucose concentration. Fig. S7 and S8† show the amperometric response for the CuI nanoflower and CuI microparticle-based electrodes, respectively. The CuI nanoplate possessed a much greater current response than the CuI nanoflower and CuI microparticle based electrode. The sensitivity and detection limit were calculated according to a previous report.[49] The calculated sensitivity for the CuI nanoplates, CuI nanoflowers and CuI microparticles were 336.05 μA mM^{-1} cm^{-2}, 24 μA mM^{-1} cm^{-2} and 13 μA mM^{-1} cm^{-2}, respectively. In comparison, the sensitivity of the CuI-nanoplates was 14 and 26 times higher than the CuI nanoflowers and CuI microparticles. The CuI nanoplates had a wider linear range than those of the CuI nanoflowers and CuI microparticles; as well, the response time for the CuI nanoplates was higher than those of the CuI nanoflowers and CuI microparticles. The non-enzymatic glucose sensing properties compared to other previous reports for non-enzymatic glucose sensors are shown in the ESI† (Table S1). Compared to the reported non-enzymatic glucose sensors, the CuI nanoplate-based sensor showed greatly improved sensitivity properties, linear range, and response time. The corresponding linear plots of calibration curves *vs.* glucose concentration for CuI nanoplates, CuI nanoflowers, and CuI microparticles are in Fig. 5b, showing the slope and linear range of the modified electrodes.

Electrochemical impedance spectroscopy (EIS) was used to inspect the interface properties of the as-prepared electrode surfaces with the CuI nanostructures. Fig. 6 represents a Nyquist diagram of the CuI nanoplates, CuI nanoflowers, and CuI microparticles in the presence of 5 mM $K_3[Fe(CN)_6]$ with

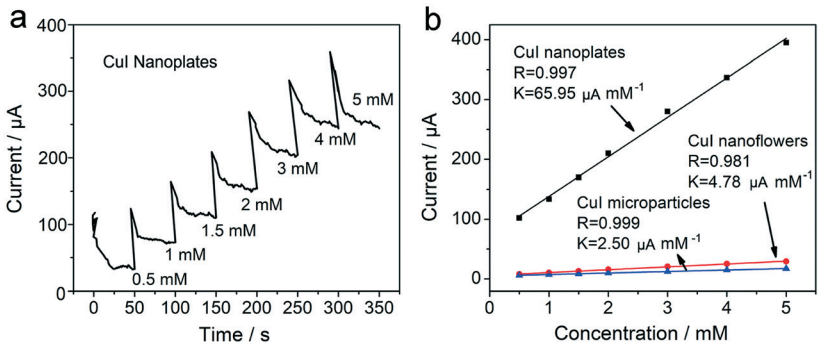

Fig. 5 (a) Amperometric current–time response of the CuI nanoplates with the addition of different concentrations of glucose ratios into 0.1 M KOH, with an applied potential of 0.62 V *vs.* Ag/AgCl. (b) The corresponding linear plots of calibration curves *vs.* glucose concentration for the CuI nanoplates, CuI nanoflowers, and CuI microparticles.

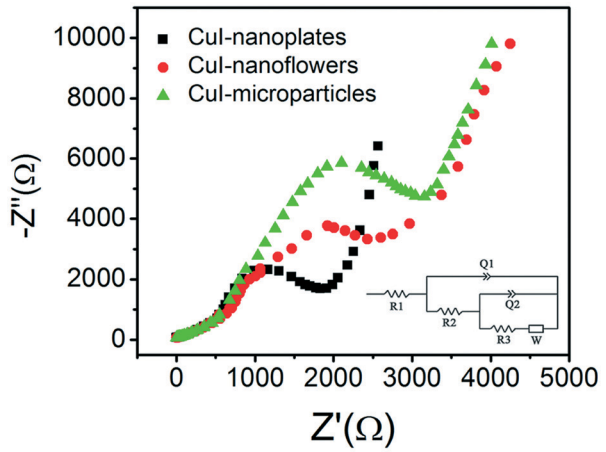

Fig. 6 Nyquist plots of the CuI nanoplates, CuI nanoflowers and CuI microstructures in the presence of 5 mM $K_3[Fe(CN)_6]$ with 0.1 M KCl as the supporting electrolyte.

0.1 M KCl as the assistant electrolyte. The plot shows two parts: one is a semicircle portion and the other is a linear portion. In these two parts, the explanation for the semicircle is due to electron transfer at higher frequencies and the other linear portion at lower frequencies results from the diffusion process.[50] The electron transfer resistance (Rct) can also be deduced from Fig. 6 by quantifying the semicircle from the Nyquist plots. The semicircle in the Nyquist plot for the CuI nanoplate/glass-carbon-electrode (GCE) indicated that the charge transfer was quite superficial, while the electrodes based on the CuI-nanoflowers and CuI microparticles showed a considerable increase in the semi-circle. This suggests that these electrodes had a steady electron and transfer delaying layer, which delay the electron transfer from the electrolyte to the surface of the electrode. It can be seen that the CuI nanoplate/GCE possessed a higher electric conductivity than those of the CuI nanoflowers and CuI microstructures, and the Rct values were around 1450 Ω, 2300 Ω and 2700 Ω, respectively. Furthermore, it confirms that the electron transfer in the CuI nanoplates is faster than those of the CuI nanoflowers and CuI microparticles.

We can conclude that the non-enzymatic glucose sensor from a CuI nanostructure is strongly dependent on the morphology and structure. The non-symmetric CuI nanoplates possess a greatly enhanced sensitivity and wide linear range. When the non-symmetric CuI nanoplates were stacked on the electrode, the smooth surface of the nanoplate increased the contact point between the CuI nanoplates, and the tooth-like surface increased the surface area which would absorb more glucose molecules from the solution. At the same time, plenty of channels formed in the piles of CuI nanoplates, due to the tooth-like morphology on one side. Thus, the molecules and ions could easily transfer in these channels. Besides the structure and morphology, the main difference of the CuI nanoplates compared the CuI nanoflowers and CuI microparticles is the specific surface area. The CuI nanoflowers can actually be regarded as the aggregation of CuI nanoplates; the specific surface area becomes smaller. For the CuI microparticles, the specific surface area became even smaller. The larger specific surface area of CuI supported more active points for sensor reactions, and at the same time increased contact with the electrode and enhanced the conductivity of the CuI nanoplates.

Conclusions

In summary, using a simple one-step synthesis method, novel non-symmetric CuI nanoplates were obtained, in which a soft template performed a key function for the formation of the non-symmetric morphology in two-dimensional space. Non-enzymatic glucose detections for CuI nanostructures have been investigated for the first time. The non-symmetric CuI nanoplate-based electrode displayed a greater sensitivity and a wider linear range than those of the CuI nanoflowers and CuI microparticles. This can be attributed to the thin and unique structural morphology of the thin CuI nanoplates with one-sided rough teeth-like peaks which enhanced the fast response in the catalytic properties of glucose sensors. The results of electrochemical impedance spectroscopy (EIS) show that the transfer of electrons in CuI nanoplates is much faster than that in CuI nanoflowers and CuI microparticles. The structural-dependent electrochemical properties of the CuI nanoplates provide a promising model for developing non-enzymatic glucose biosensors.

Conflicts of interest

There are no conflicts to declare.

Acknowledgements

H. J. You acknowledges the programs supported by the Natural Science Foundation of Shaanxi Province (No. 2017JM5072), and the Fundamental Research Funds for the Central Universities (No. xjj2017102). J. X. Fang acknowledges the programs supported by the National Natural Science Foundation of China (No. 21675122, 21874104), the Key Research Program in Shaanxi (2017NY-114), the World-Class Universities (Disciplines) and the Characteristic Development Guidance Funds for the Central Universities.

Notes and references

1 Y. Lin, P. Yu, J. Hao, Y. Wang, T. Ohsaka and L. Mao, *Anal. Chem.*, 2014, **86**, 3895.
2 D. Odaci, B. N. Gacal, B. Gacal, S. Timur and Y. Yagci, *Biomacromolecules*, 2009, **10**, 2928.
3 J. Kropff, D. Bruttomesso, W. Doll, A. Farret, S. Galasso, Y. M. Luijf, J. K. Mader, J. Place, F. Boscari, T. R. Pieber, E. Renard and J. H. DeVries, *Diabetes, Obes. Metab.*, 2015, **17**, 349.
4 K. Benassi, J. Drobny and T. Aye, *Diabetes Technol. Ther.*, 2013, **15**, 409.

5 L. Guariguata, D. R. Whiting, I. Hambleton, J. Beagley, U. Linnenkamp and J. E. Shaw, *Diabetes Res. Clin. Pract.*, 2014, **103**, 137–149.
6 P. K. Kannan and C. S. Rout, *Chem. – Eur. J.*, 2015, **21**, 9355.
7 J. Wang, *Chem. Rev.*, 2008, **108**, 814.
8 Q. Zheng, B. J. Shi, F. R. Fan, X. X. Wang, L. Yan, W. W. Yuan, S. H. Wang, H. Liu, Z. Li and Z. L. Wang, *Adv. Mater.*, 2014, **26**, 5856.
9 P. H. Yeh, Z. Li and Z. L. Wang, *Adv. Mater.*, 2009, **21**, 4978.
10 H. O. Yang, J. J. Tian, G. L. Sun, Y. Zou, Z. Liu, H. Li, L. M. Zhao, B. J. Shi, Y. B. Fan, Y. F. Fan, Z. L. Wang and Z. Li, *Adv. Mater.*, 2017, **29**, 1703456.
11 Z. Liu, L. Cheng, L. Zhang, C. Jing, X. Shi, Z. B. Yang, Y. T. Long and J. X. Fang, *Nanoscale*, 2014, **6**, 2572.
12 J. X. Fang, H. Hahn, R. Krupke, F. Schramm, T. Scherer, B. J. Ding and X. P. Song, *Chem. Commun.*, 2009, 1132.
13 C. F. Tian, Y. H. Deng, D. Y. Zhao and J. X. Fang, *Adv. Opt. Mater.*, 2015, **3**, 411.
14 Y. Liu, S. Liu, R. Chen, W. Zhan, H. Ni and F. Liang, *Electroanalysis*, 2015, **27**, 1138.
15 P. W. Barone, R. S. Parker and M. S. Strano, *Anal. Chem.*, 2005, **77**, 7556.
16 Z. Cheng, E. Wang and X. Yang, *Biosens. Bioelectron.*, 2001, **16**, 179.
17 M. Liu, R. Liu and W. Chen, *Biosens. Bioelectron.*, 2013, **45**, 206.
18 J. Wang and W. D. Zhang, *Electrochim. Acta*, 2011, **56**, 7510.
19 Y. Lin, F. Lu, Y. Tu and Z. Ren, *Nano Lett.*, 2004, **2**, 191.
20 Z. Li, Y. Xin, Z. Zhang, H. Wu and P. Wang, *Sci. Rep.*, 2015, **5**, 10617.
21 C. Li, M. Kurniawan, D. Sun, H. Tabata and J. J. Delauna, *Nanotechnology*, 2015, **26**, 015503.
22 Y. Li, Y. Zhong, Y. Zhang, W. Weng and S. Li, *Sens. Actuators, B*, 2015, **206**, 735.
23 J. Lv, C. C. Kong, Y. Xu, Z. M. Yang, X. J. Zhang, S. C. Yang, G. Meng, J. L. Bi, J. H. Li and S. Yang, *Sens. Actuators, B*, 2017, **248**, 630.
24 H. Q. Feng, C. C. Zhao, P. C. Tan, R. P. Liu, X. Chen and Z. Li, *Adv. Healthcare Mater.*, 2018, 1701298.
25 B. J. Shi, Z. Li and Y. Fan, *Adv. Mater.*, 2018, 1801511.
26 X. Kang, Z. Mai, X. Zou, P. Cai and J. Mo, *Talanta*, 2008, **74**, 879.
27 H. Bai, M. Han, Y. Du, J. Bao and Z. Dai, *Chem. Commun.*, 2010, **46**, 1739.
28 T. K. Huang, K. W. Lin, S. P. Tung, T. M. Cheng, I. C. Chang, Y. Z. Hsieh, C. Y. Lee and H. T. Chiu, *J. Electroanal. Chem.*, 2009, **636**, 123.
29 X. C. Dong, H. Xu, X. W. Wang, Y. X. Huang, M. B. Chan-Park, H. Zhang, L. H. Wang, W. Huang and P. Chen, *ACS Nano*, 2012, **6**, 3206.
30 X. Wang, Y. Zhang, C. E. Banks, Q. Chen and X. Ji, *Colloids Surf., B*, 2010, **78**, 363.
31 S. S. Mahshid, S. Mahshid, A. Dolati, M. Ghorbani, L. Yang, S. Luo and Q. Cai, *Electrochim. Acta*, 2011, **58**, 551.
32 L. Y. Chen, T. Fujita, Y. Ding and M. W. Chen, *Adv. Funct. Mater.*, 2010, **20**, 2279.
33 Y. Ding, Y. Liu, L. Zhang, Y. Wang, M. Bellagamba, J. Parisi, C. M. Li and Y. Lei, *Electrochim. Acta*, 2011, **58**, 209.
34 H. J. Kim, J. H. Jun, H. J. Choi, H. Kwon, J. Park, C. W. Seo, J. K. Kim, J. H. Shin, J. Y. Kim, H. Lee and J. M. Baik, *Nano Energy*, 2018, **53**, 474.
35 I. G. Mbomson, S. McMeekin, B. Lahiri, R. D. L. Rue and N. P. Johnson, *Proc. SPIE*, 2014, **12**, 2052578.
36 E. H. Khoo, E. S. P. Leong, S. J. Wu, W. K. Phua, Y. L. Hor and Y. J. Liu, *Sci. Rep.*, 2016, **6**, 1965.
37 Y. H. Zang, J. Yin, X. He, C. Yue, Z. Wu, J. Li and J. Kang, *J. Mater. Chem. A*, 2014, **2**, 7753.
38 Y. Y. Yang and L. X. Zhang, *J. Russ. Laser Res.*, 2018, **39**, 274.
39 M. U. Khan, H. J. You, X. T. Liu, L. L. Zhang and J. X. Fang, *Small*, 2018, **14**, 1702948.
40 F. Li, Y. Ding, X. Gao, X. Q. Xin and Z. L. Wang, *Angew. Chem., Int. Ed.*, 2004, **43**, 5238.
41 J. X. Fang, J. Li, C. F. Tian, Q. Q. Gao, X. J. Wang, N. Y. Gao, X. L. Wen, C. S. Ma, H. J. You, Z. L. Yang, Q. H. Xu, Q. H. Xiong and Z. Y. Li, *NPG Asia Mater.*, 2016, **8**, e323.
42 H. J. You, F. L. Zhang, Z. Liu and J. X. Fang, *ACS Catal.*, 2014, **4**, 2829.
43 Z. B. Yang, L. Zhang, H. J. You, Z. Y. Li and J. X. Fang, *Part. Part. Syst. Charact.*, 2014, **31**, 390.
44 H. J. You and J. X. Fang, *Nano Today*, 2016, **11**, 145.
45 H. J. You, S. C. Yang, B. J. Ding and H. Yang, *Chem. Soc. Rev.*, 2013, **42**, 2880.
46 S. Felix, P. Kollu, B. P. Raghupathy, S. K. Jeong and A. N. Grace, *J. Chem. Sci.*, 2014, **126**, 25.
47 J. Song, L. Xu, C. Zhou, R. Xing, Q. Dai, D. Liu and H. Song, *ACS Appl. Mater. Interfaces*, 2013, **5**, 12934.
48 N. Lu, C. Shao, X. Li, T. Shen, M. Zhang, F. Miao, P. Zhang, X. Zhang, K. Wang and Y. Zhang, *RSC Adv.*, 2014, **4**, 31056.
49 H. Wei, J. Sun, L. Guo, X. Li and G. Chen, *Chem. Commun.*, 2009, 2842.
50 X. Kang, J. Wang, H. Wu, I. A. Aksay, J. Liu and Y. Lin, *Biosens. Bioelectron.*, 2009, **25**, 901.